Three-magnon processes in magnetic nanoelements: Quantization and localized mode effects

R. E. Camley

Center for Magnetism and Magnetic Nanostructures, University of Colorado at Colorado Springs, Colorado Springs, Colorado 80918, USA

(Received 13 November 2013; revised manuscript received 28 March 2014; published 2 June 2014)

Three-magnon effects are known to be important for nonlinear processes in magnetic thin films. In such a process, for example, the uniform mode at a frequency ω can decay into two modes at a lower frequency $\omega/2$. In magnetic nanoelements, there are additional concerns which do not occur in films. First, in small elements, the excitation wave vectors become a set of discrete values. This limits the availability of final states. Second, localized modes are important in nanoelements. Our study is based on micromagnetic calculations using the Landau-Lifshitz equations. We use an oscillating magnetic field at frequency ω to drive the system and to study the response over a wide range of frequencies and for a wide set of input powers. In nanoelements, the typical response occurs not exactly at $\omega/2$ but for several frequencies which are symmetrically spaced around $\omega/2$. This is explained by the two considerations introduced above. We study the response both as a function of the amplitude of the driving field and as a function of the driving frequency. In this way, we can study the system response both at resonance and outside of resonance.

DOI: 10.1103/PhysRevB.89.214402 PACS number(s): 76.50.+g, 75.75.−c, 75.78.−n, 75.30.Ds

I. INTRODUCTION

Nonlinear magnetic dynamics have been an important research topic for many years [1–9], however, most of the earlier experimental studies were limited to large samples of yttrium iron garnet because of its low linewidth. With recent developments in thin-film creation and structuring, it has become possible to extend these studies to new materials, such as ferromagnetic metals [10–20], and new structures including ultrathin films and nanoelements.

The equations of motion for the magnetization are inherently nonlinear, and studies of nonlinear objects, such as solitons, have been researched substantially. Nonlinear processes in magnetic materials can also lead to a number of interesting effects for waves. For example, a single input wave at frequency ω can result in output waves at the harmonics [10,18] of ω, 2ω, 3ω, 4ω, etc. In addition, one can mix two input waves with frequencies ω_1 and ω_2 to produce output waves with frequencies of $2\omega_1 + \omega_2$ or $2\omega_1 - \omega_2$, for example, see Refs. [10,15,18,20].

In this paper, we study a different nonlinear mechanism, the three-magnon process, that can give rise to very different output waves. In such a process, for example, the uniform mode at a frequency ω can decay into two modes at a lower frequency $\omega/2$. Such three-magnon effects are known to be important for the so-called saturation of the ferromagnetic resonance (FMR) [2]. These processes can also be important for signal processing or magnetic logic applications.

The existence of these lower-frequency modes in a thin film depends on the so-called backward-volume-magnetostatic waves where the frequency of the modes decreases as the wave vector increases. Here we study three-magnon processes, theoretically, in magnetic nanoelements [21–28] and find that two important new considerations occur:

(1) In small elements, the wave vector becomes a set of discrete values. This limits the availability of states at the frequency of $\omega/2$ because the frequency also becomes a set of discrete values.

(2) Localized modes are important in nanoelements. These modes often have low frequencies and provide a mechanism for a decay from ω to $\omega/2$ that does not involve the usual magnetostatic waves that one finds in extended films.

Our study is based on micromagnetic calculations using the Landau-Lifshitz (LL) equations. We use an input wave at a frequency ω and study the response of the system over a wide range of frequencies and for a wide set of input powers. Our results show that a typical response occurs not exactly at $\omega/2$ but for several pairs of frequencies which are symmetrically spaced around $\omega/2$. This is explained by the two considerations introduced above.

II. THEORETICAL CONSIDERATIONS

We first review the typical three-magnon decay process for the uniform mode in ferromagnetic resonance in an extended film. The uniform mode is characterized by a wave vector $\mathbf{k} = 0$ and a frequency ω. The three-magnon decay process depends on the availability of modes at a frequency of $\omega/2$. Figure 1 shows the dispersion curves for the different standing spin-wave modes in a thin film of thickness 275 nm for propagation parallel to the applied field. The parameters for this plot are applied field $H = 500$ Oe and saturation magnetization $M = 0.76$ kG, gyromagnetic ratio $\gamma = 2.85$ GHz/kOe, and exchange stiffness constant $D = 1.1\times10^{-12}$ kG cm^2. (Using $A = DM_s/2$, this is equivalent to an exchange constant $A = 4.18\times10^{-7}$ erg/cm, somewhat reduced from the value used later of $A = 1.3\times10^{-6}$ erg/cm, which typically is used in micromagnetic calculations. The reduced value of exchange here allows us to see the general features more easily.) The curves are calculated using the methods developed in Ref. [29]. Recently, these methods have been checked against micromagnetic simulations with good agreement [30].

In the example shown here, there clearly are modes below the half-frequency value, and one could expect a three-magnon decay to be possible. One only needs to satisfy conservation of energy and momentum. If the system is driven by a spatially uniform oscillating magnetic field at frequency ω_o, then these

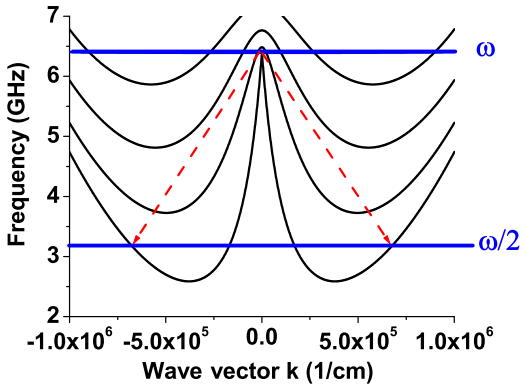

FIG. 1. (Color online) Dipole-exchange modes in a thin film for propagation parallel to the applied field. The dashed lines indicate a possible decay from the uniform mode ($\mathbf{k} = 0$) to two half-frequency modes. The parameters (given in the text) are appropriate for a 275-nm-thick Permalloy film in an external field of 500 Oe.

conditions are as follows:

$$\hbar\omega_o = \hbar\omega_1 + \hbar\omega_1, \tag{1}$$

$$0 = \hbar k_1 + -\hbar k_1, \tag{2}$$

where ω_o is the FMR frequency and $\omega_1 = \omega_o/2$. Similarly, in Eq. (2), the initial momentum for the uniform FMR mode is 0, and the momentum for one of the states to which the FMR mode decays is given by $\hbar k_1$. A decay possibility that satisfies all these conservation rules is shown by the dashed lines in Fig. 1.

Of course, the propagation direction does not have to be parallel to the applied field. At other angles of propagation, there are also modes which will satisfy these two conditions. We do note that, as the angle between the propagation wave vector and the external static field gets larger, the frequencies generally are pushed up to larger values and, thus, half-frequency modes are no longer available.

With these ideas in mind, one would expect that, if the system is driven at a frequency ω, there could be a response at ω and a nonlinear response at $\omega/2$. In fact, it is not quite so simple; it is well known that there is a threshold value for the driving field and that only above this value will there be a response at $\omega/2$. We will see that our numerical results for nanosized elements are actually quite different. While there is a threshold field, the typical response is not at ω but exists at multiple pairs of frequencies which are symmetrically spaced around $\omega/2$.

The dynamic micromagnetic calculation uses the LL equation to find the magnetization of each of the cells as it evolves through time. The method is similar to that used in OOMMF [31]. The LL equation is as follows:

$$\frac{\partial \vec{M}}{\partial t} = -|\gamma|(\vec{M} \times \vec{H}_{\text{eff}}) - |\gamma|\frac{\alpha}{M_s}\vec{M}\times(\vec{M}\times\vec{H}_{\text{eff}}), \tag{3}$$

where $\vec{M}$ is the magnetization of the cell and $\vec{H}_{\text{eff}}$ is the effective magnetic field present in the cell and is given by

$$\vec{H}_{\text{eff}} = \vec{H}_0 + \vec{H}_{\text{ex}} + \vec{H}_{\text{dip}} + h_d\cos(\omega t)\hat{y}, \tag{4}$$

where $\vec{H}_0$ is the external static magnetic field in the z direction, $\vec{H}_{\text{ex}}$ is the effective exchange field between nearest-neighbor cells, $\vec{H}_{\text{dip}}$ includes the dipole fields created from all cells including the single cell's own demagnetizing field, and $h_d \cos(\omega t)\,\hat{y}$ is the driving field from the microwave field when it is present. The dipole field is calculated efficiently through a standard fast Fourier transform (FFT) method.

The coupled set of magnetic cells is driven with an oscillating field h_d at a given frequency ω_d. To measure the response, one can calculate the Fourier transform of the time evolution of the magnetization using a FFT method. There are a number of ways to do this for a multisite system. One way is to first find the average magnetization for the structure as a whole as a function of time and then do the FFT. For example, the average value for the magnetization in the x direction is given by

$$\bar{m}_x(t) = \sum_{\text{all cells } i} m_x^{(i)}(t). \tag{5}$$

The Fourier transform of this would be

$$\bar{m}_x(\omega) = F[\bar{m}_x(t)]. \tag{6}$$

This would result in a series of peaks in the frequency space where the peaks typically occur near the nonlinearly generated waves of the system. Of course, one would expect that the largest peak occurs at the driving frequency ω_d. In fact, there are also peaks at harmonics of the driving frequency. This has recently been examined both experimentally and theoretically. The first method is good for understanding how the system, as a whole, responds to a uniform oscillating field, for example. But a spatially odd spin wave will not be seen in this because the motion in one cell will be canceled out by the spin motion somewhere else in the system during the averaging.

In contrast, one can first perform a FFT on the time evolution of the spin motion in each cell and then average the FFT amplitude values over all cells. This method does not suffer from the cancellation issues in the first method, and both even and odd modes are seen. Because of this, the second method gives more information on the nonlinear response, and we will use this method in what follows. In terms of experimental measurements, a technique, such as the standard ferromagnetic resonance, measures the behavior of the average magnetization. However, there are localized techniques, such as microfocused Brillouin light scattering [32–34], which can measure excitations in a portion of a nanoparticle, and they would be appropriate for measurements that are related to the localized Fourier transforms discussed here.

III. RESULTS

The geometry is illustrated in Fig. 2. The sample lies in the yz plane, and a static magnetic field $H = 1$ kOe is applied at a slight misalignment (0.1°) from the long axis of the nanoparticle in the plane of the nanoparticle. The misalignment prevents any numerical problems that sometimes occur in highly symmetric situations. Furthermore, in real systems, it is impossible to align the magnetic field perfectly with the nanoparticle axis. In addition, there is a microwave driving field h_d, which is along the y axis.

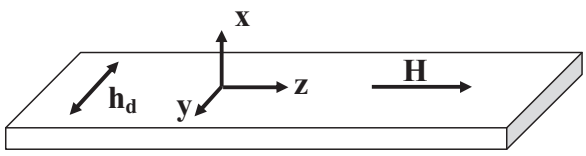

FIG. 2. The geometry used in this paper. A rectangular nanoelement has its long axis in the z direction. There is an applied static magnetic field H applied in the zy plane at an angle of 0.1° away from the z axis. An oscillating field h_d is applied in the y direction.

We use the second method outlined above to characterize the response of a nanoelement with dimensions 320 nm×640 nm×100 nm to a single driving frequency. Figure 3 shows the frequency response of the system for driving fields h_d with different amplitudes but all at a frequency of 12.46 GHz. For this calculation, the parameters are—cell size = 5 nm×5 nm×100 nm, number of cells = 64×128×1, saturation magnetization $M_s = 763.9$ G, exchange constant $A = 1.3\times10^{-6}$ erg/cm, and damping constant $\alpha = 0.02$. The frequency resolution resulting from the FFT transform is 0.01 GHz. The system is brought to an equilibrium state, in this case, a nearly saturated state generally known as a "flower state" before the oscillating field is introduced. After the driving field is turned on, we wait about 5 ns to achieve dynamic equilibrium before data collection for the FFT is turned on.

We have performed a number of checks to see that our results do not depend significantly on cell size. For example, using a unit cell of 10 nm×10 nm×100 nm and reducing the number of cells give, essentially, the same results. We have also reduced the cell size for the thickness to 50 nm and doubled the number of cells with the same general results emerging. The key results seen in Fig. 3 are as follows:

(1) At low amplitude driving fields, the only substantial response is at the driving field. All other responses are several orders of magnitude smaller.

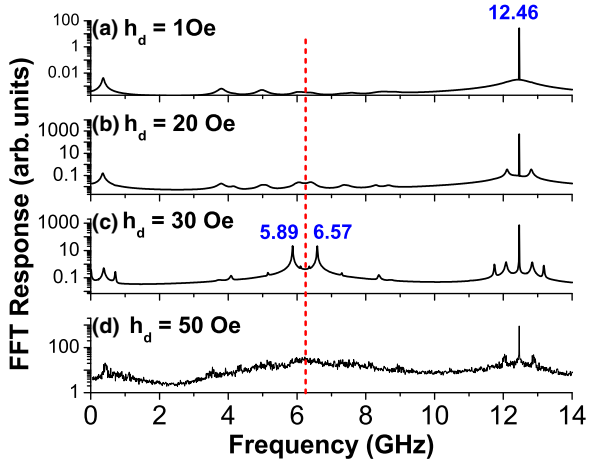

FIG. 3. (Color online) The excitation spectrum of a 320 nm× 640 nm×100 nm Permalloy bar when driven at 12.46 GHz with driving fields of different amplitudes. There is a static applied field of 1 kOe in the z direction. The dashed line shows the half-frequency position. A pair of symmetrically spaced peaks (around the half frequency) is visible at a driving field of 30 Oe.

(2) At a higher amplitude for the driving field ($h_d = 30$ Oe), one sees a peak at the driving field and several sets of peaks which are equidistant in frequency from the half-frequency point $\omega/2$.

(3) At even higher amplitudes, one sees numerous small peaks throughout the entire frequency range. The individual peaks rest on a background which shows a broad peak near $\omega/2$.

We can understand the general trends of these results by examining a version of Fig. 1 showing the dipole-exchange modes but now adjusted for a finite structure. First, as noted above, in small elements, the wave vector is quantized. Here, as an illustration, we assume that the quantized wave vectors in the horizontal plane are given by $q_z = \pm n\pi/L_z$, where L_z is the length of the nanoelement in the z direction and n is an integer. Second, in finite systems, it is not appropriate to have a mode characterized by $+q_z$ or by $-q_z$. Because of reflections at the edges, all the modes are essentially standing modes and contain both positive and negative wave-vector contributions.

Because of the two features discussed above, the conservation of energy and momentum rules discussed above become modified. We can now have a three-magnon process where an initial spatially uniform mode ($\mathbf{k} = 0$) with a frequency ω_o mode decays to two modes, one at frequency $\omega_o/2 + \Delta\omega$ and one at $\omega_o/2 - \Delta\omega$. This conserves energy because

$$\hbar\omega_o = \hbar\left(\frac{\omega_o}{2} + \Delta\omega\right) + \hbar\left(\frac{\omega_o}{2} - \Delta\omega\right). \tag{7}$$

For this process to occur, there must be two states spaced equally (in frequency) about $\omega_o/2$. Because the dispersion relation is no longer continuous, this is not guaranteed and only happens at a few special points. The process also conserves momentum because the initial wave vector has $\mathbf{k} = 0$ and the total final wave vector is also zero because of the finite structure. (Each state now has both $+\mathbf{k}$ and $-\mathbf{k}$ components). This new set of decay possibilities is illustrated in Fig. 4. It is this new set of conservation rules that leads to the peaks in the

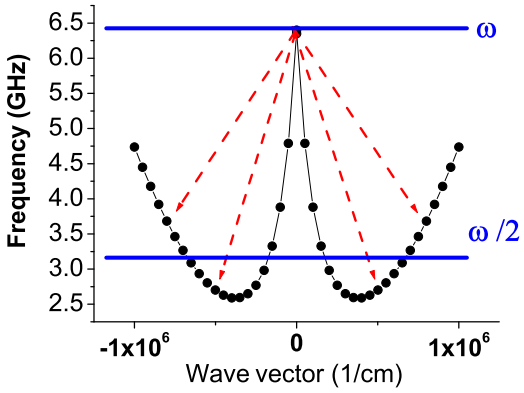

FIG. 4. (Color online) The lowest-frequency dipole-exchange mode in a nanoelement for propagation parallel to the applied field. The parameters (given in the text) are appropriate for a 275-nm-thick Permalloy film in an external field of 500 Oe. The finite length of the rectangular ribbon is 617 nm leading to a discretization of the allowed wave vectors. The dashed lines indicate possible decays from the uniform mode ($\mathbf{k} = 0$) to two modes equally spaced about the half-frequency position.

FFT spectrum which are equally spaced in frequency about the $\omega/2$ value.

We note that, in the absence of translational invariance where the absence here is caused by the finite size of the sample, there is technically no requirement for conservation of momentum. However, in large samples, the concept of momentum conservation is useful, and it continues to be conceptually useful as we begin to make the samples smaller. Nonetheless, the idea that all spin-wave modes are standing waves implies that, essentially, all modes have a total momentum of zero, i.e., the sum of the wave vectors for a given mode is zero.

The true situation is not as simple as this in nanoelements, and the modes do not exactly follow the quantization outlined above, nor do they exactly follow the frequencies predicted by the dipole-exchange calculation. First, dynamic pinning of the modes alters the allowed wavelengths. Also, the static and dynamic demagnetizing fields in a nanoelement are different from those in the extended film, and this alters the frequency somewhat, particularly for the uniform mode (where $q = 0$), which is shifted up by about 1 GHz from the dipole-exchange value. Nonetheless, the simple quantization picture gives some good insight into why the new peaks in the FFT spectrum are distributed symmetrically around $\omega/2$ rather than at $\omega/2$ and why there is a relatively small number of these peaks. We note that a related discussion on the width of the $\omega/2$ magnon peak in Brillouin light-scattering experiments has been given earlier [35].

We comment on the issue of resonance for these results. In experiments, it is common to set the driving frequency at a resonant frequency of the system. This is normally performed to ensure a large response. However, in the nonlinear limit, the resonance frequency changes as a function of the amplitude of the driving field [14]. So, it is impossible to set a single resonance frequency and have it valid for all driving fields. Nonetheless, it is interesting to see how the response of the system changes as a function of frequency and, in particular, in the regions where the driving frequency is close to the resonance frequency.

Figure 5 explores the response of the nanoparticle where the driving amplitude is held constant but the frequency is changed. The geometry of the system is the same as that used in Fig. 3. With a static field of 1 kOe applied along the long axis, the resonance frequency in the linear limit is estimated to be around 12.6 GHz. In Fig. 5(a), the driving frequency is 11.8 GHz, relatively far away from resonance, and there is no significant response near the $\omega/2$ frequency. In contrast, in Fig. 5(b) where the frequency is 12 GHz, there are two sharp peaks, symmetrically spaced around the $\omega/2$ frequency. At 12.6 GHz, in Fig. 5(c), we see a significant set of responses throughout the frequency range, but many are symmetrically spaced around $\omega/2$. Finally, at a frequency well away from resonance at 13.2 GHz [Fig. 5(d)], the response is quite small except at the driving frequency. It is clear from this figure that, as the driving frequency approaches the resonance frequency, the response of the system gets larger as expected and that the symmetric spacing of the modes around $\omega/2$ exists for a range of frequencies, not just for the resonance frequency.

It is interesting to note that many of the peaks in Fig. 5(c) can simply be explained by other nonlinear processes. We identify the main peaks in Fig. 5(c) as $\omega_o = 12.6$, $\omega_1 = 5.91$,

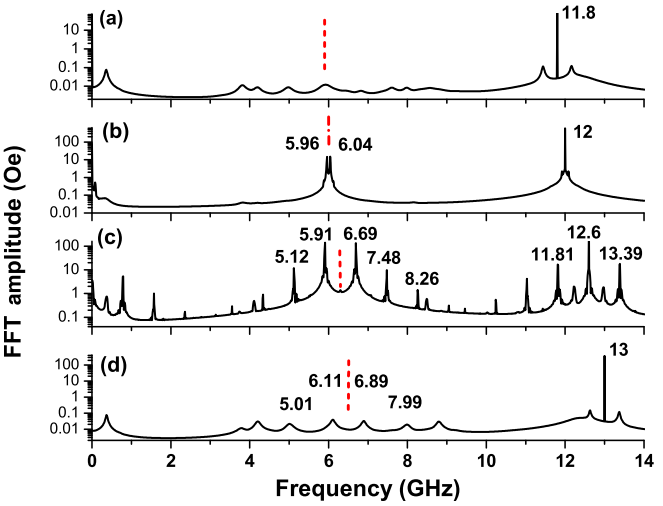

FIG. 5. (Color online) The excitation spectrum of a 320 nm× 640 nm×100 nm Permalloy bar when driven at different frequencies. The driving field has an amplitude of 30 Oe. There is a static applied field of 1 kOe in the z direction. The dashed lines show the half-frequency positions. The frequency of 12.6 is close to the resonance field. Some peaks are labeled with their frequencies in gigahertz.

and $\omega_2 = 6.69$ GHz. Many of the other peaks come from the allowed nonlinear combinations of these three modes. For example, the peaks at 5.12 and 7.48 GHz result from $2\omega_1 - \omega_2$ and $2\omega_2 - \omega_1$ processes, respectively. Then the frequencies of 6.69 and 7.48 GHz can be combined similarly to produce the peak at 8.26 GHz. The peaks at 11.81 and 13.39 GHz are the second harmonics of ω_1 and ω_2. Many of the remaining modes can be identified in a similar fashion as arising directly from combinations of ω_o, ω_1, or ω_2 or from combinations of these frequencies with the frequencies they generate. Finally, we note that, in addition to the identified satellite peaks around $\omega/2$, there are often other satellite peaks surrounding the strong peak at the driving frequency. These seem to be associated with a nonlinear generated combination of the driving frequency and the lowest-frequency peak that is probably an edge mode with a long lifetime.

We can get some idea of the nature of the waves which are involved in the three-magnon process by making a "snapshot" of the mode. This is performed by finding the amplitude of the Fourier transform of the transverse magnetization, in this case M_y, in each cell at a specified frequency. Figure 6 shows the profiles for the two modes near $\omega/2$ seen in Fig. 5(c) at frequencies of 5.91 and 6.69 GHz. It is clear from these figures that both modes show some localization, i.e., the amplitude is larger at the ends of the nanoelement, in contrast to the uniform amplitude expected from a sinusoidal standing wave. The localized modes may not have well defined $\mathbf{k}$ vectors. For example, a Fourier transform of the spatial pattern would show some peaks at specific wave vectors as well as broader background structures. Nonetheless, because it is a standing mode, one expects that the total wave vector will continue to be zero. The mode at 5.91 GHz has minimal variation in the y (horizontal) direction and $\mathbf{k}_y \approx 0$. In contrast, the mode at 6.69 GHz has a node in the excitation as one moves along the y axis and $\mathbf{k}_y \approx \pi/L_y$.

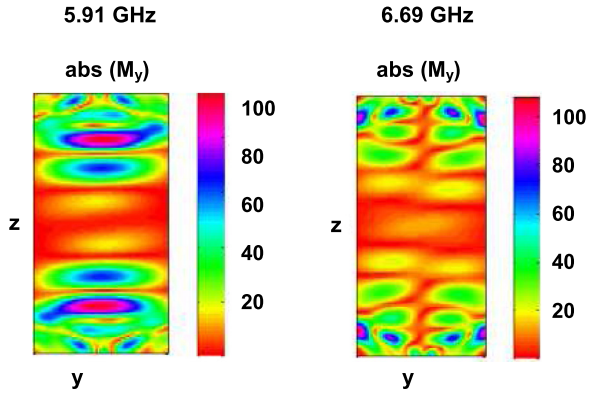

FIG. 6. (Color online) A spatial representation of the excitations at 5.91 and 6.69 GHz using the parameters from Fig. 5(c). The colors show the amplitude of the excitation, obtained through the FFT, for the different frequencies. The excitations clearly show some localization in that the amplitudes are smaller in the center of the bar.

It is important to note that the existence of the three-magnon process depends critically on the dimensions of the nanoelement. For example, as is well known for thin films, the size of the dip seen in the dispersion relation shown in Figs. 1 and 4 depends on both the magnetic field and the thickness of the film. As the film is made thinner, the dip is reduced, and there may be no modes with frequencies as low as $\omega/2$. We find a similar result in our numerical studies. For example, we found no three-magnon-like processes in a nanoelement with a 10-nm thickness. In nanoelements, other considerations are also important. If one has a nanoelement with a square cross section, this creates an effective anisotropy field (from the dynamic demagnetizing fields), which acts like an external field pointing along the long axis of the nanoelement. This field makes it harder to get large-amplitude oscillations, and thus, the nonlinear regime requires very large driving fields with amplitudes of over 100 Oe. Thus, nonlinear effects and, in particular, three-magnon effects are difficult to obtain in this limit. This also matches with our numerical results.

IV. SUMMARY

We have studied the nonlinear decay processes of a rectangular magnetic nanoelement when driven by an oscillating, but spatially uniform, microwave field at frequency ω. In particular, the three-magnon process, which, in thin films, leads to waves at $\omega/2$, produces a different result in nanoelements, leading to responses at several frequencies which are symmetrically spaced around $\omega/2$. When the driving field is large and near the resonance frequency for the uniform mode, the excitation spectrum can be quite complicated. However, many of the peaks seen in that spectrum result from nonlinear combinations of the original wave and the three-magnon waves which are spaced around $\omega/2$.

ACKNOWLEDGMENT

This work was funded by NSF Grant No. DMR 0907063. The author would like to thank J. Marsh for carrying out some of the numerical calculations.

[1] N. Bloembergen and R. W. Damon, Phys. Rev. **85**, 699 (1952).
[2] H. Suhl, Phys. Rev. **101**, 1437 (1956); J. Phys. Chem. Solids **1**, 209 (1957).
[3] C. E. Patton, Phys. Rep. **103**, 251 (1984).
[4] B. A. Kalinikos, N. G. Kovshikov, and C. E. Patton, Phys. Rev. Lett. **80**, 4301 (1998).
[5] M. Wu, B. A. Kalinikos, and C. E. Patton, Phys. Rev. Lett. **95**, 237202 (2005).
[6] *Nonlinear Phenomena and Chaos in Magnetic Materials*, edited by P. E. Wigen (World Scientific, Singapore, 1994).
[7] S. O. Demokritov, B. Hillebrands, and A. Slavin, Phys. Rep. **348**, 441 (2001).
[8] G. Bertotti, I. D. Mayergoyz, and C. Serpico, *Nonlinear Magnetization Dynamics in Nanosystems* (Elsevier, Amsterdam, 2009).
[9] K. Livesey, R. L. Stamps, and M. Kostylev, Phys. Rev. B **75**, 174427 (2007).
[10] M. Bao, A. Khitun, Y. Wu, J.-Y. Lee, K. L. Wang, and A. P. Jacob, Appl. Phys. Lett. **93**, 072509 (2008).
[11] C. Cheng and W. E. Bailey, Appl. Phys. Lett. **103**, 242402 (2013).
[12] H. M. Olson, P. Krivosik, K. Srinivasan, and C. E. Patton, J. Appl. Phys. **102**, 023904 (2007).
[13] M. Yan, P. Vavassori, G. Leaf, F. Y. Fradin, and M. Grimsditch, J. Magn. Magn. Mater. **320**, 1909 (2008).
[14] Y. Khivintsev, B. Kuanr, T. J. Fal, M. Haftel, R. E. Camley, Z. Celinski, and D. L. Mills, Phys. Rev. B **81** 054436 (2010).
[15] Y. Khivintsev, J. Marsh, V. Zagorodnii, I. Harward I, J. Lovejoy, P. Krivosik, R. E. Camley, and Z. Celinski, Appl. Phys. Lett. **98**, 042505 (2011).
[16] H. Ulrichs, V. E. Demidov, S. O. Demokritov, and S. Urazhdin, Phys. Rev. B **84**, 094401 (2011).
[17] C. T. Boone, J. A. Katine, J. R. Childress, V. Tiberkevich, A. Slavin, J. Zhu, X. Cheng, and I. N. Krivorotov, Phys. Rev. Lett. **103**, 167601 (2009).
[18] J. Marsh, V. Zagorodnii, Z. Celinski, and R. E. Camley, Appl. Phys. Lett. **100**, 102404 (2012).
[19] M. P. Wismayer, B.W. Southern, X. L. Fan, Y. S. Gui, C.-M. Hu, and R. E. Camley, Phys. Rev. B **85**, 064411 (2012).
[20] J. Marsh and R. E. Camley, Phys. Rev. B **86**, 224405 (2012).
[21] K. Y. Guslienko, S. O. Demokritov, B. Hillebrands, and A. N. Slavin, Phys. Rev. B **66**, 132402 (2002).
[22] M. Grimsditch, G. K. Leaf, H. G. Kaper, D. A. Karpeev, and R. E. Camley, Phys. Rev. B **69**, 174428 (2004).
[23] R. D. McMichael and M. D. Stiles, J. Appl. Phys. **97**, 10J901 (2005).
[24] V. E. Demidov, M. Buchmeier, K. Rott, P. Krzysteczko, J. Münchenberger, G. Reiss, and S. O. Demokritov, Phys. Rev. Lett. **104**, 217203 (2010).

[25] V. E. Demidov, U.-H. Hansen, and S. O. Demokritov, Phys. Rev. Lett. **98**, 157203 (2007).
[26] V. S. Tiberkevich, J.-V. Kim, and A. N. Slavin, Phys. Rev. B **78**, 092401 (2008).
[27] Y. S. Gui, N. Mecking, X. Zhou, G. Williams, and C.-M. Hu, Phys. Rev. Lett. **98**, 107602 (2007); Y. S. Gui, N. Mecking, and C.-M. Hu, *ibid.* **98**, 217603 (2007).
[28] Y. S. Gui, A. Wirthmann, N. Mecking, and C.-M. Hu, Phys. Rev. B **80**, 060402(R) (2009); **80**, 184422 (2009).
[29] T. Wolfram and R. E. DeWames, Prog. Surf. Sci. **2**, 233 (1972).
[30] E. Meloche, J. I. Mercer, J. P. Whitehead, T. M. Nguyen, and M. L. Plumer, Phys. Rev. B **83**, 174425 (2011).
[31] M. J. Donahue and D. G. Porter, National Institute of Standards and Technology, Interagency Report No. NISTIR6376, 1999 (unpublished).
[32] M. Madami, G. Gubbiotti, S. Tacchi, and G. Carlotti, in *Solid State Physics*, edited by R. E. Camley and R. L. Stamps (Academic, Burlington, MA, 2012), Vol. 63, pp. 79–150.
[33] D. R. Birt, B. O'Gorman, M. Tsoi, X. Li, V. E. Demidov, and S. O. Demokritov, Appl. Phys. Lett. **95**, 122510 (2009).
[34] H. Ulrichs, V. E. Demidov, S. O. Demokritov, A. V. Ognev, M. E. Stebliy, L. A. Chebotkevich, and A. S. Samardak, Phys. Rev. B **83**, 184403 (2011).
[35] C. L. Ordóñez-Romero, B. A. Kalinikos, P. Krivosik, W. Tong, P. Kabos, and C. E. Patton, Phys. Rev. B **79**, 144428 (2009).